Article

Validation of AISI Design of Cold-Formed Steel Beams Using Non-Linear Finite Element Analysis

Muhammad Ali Khan [1,*], Rehan Farid Mustafa [1], Zahid Ahmad Siddiqi [1] and Rehan Masood [2,*]

[1] Department of Civil Engineering, The University of Lahore, Lahore 54590, Pakistan; rehanfarid7@gmail.com (R.F.M.); zahid.siddiqi@ce.uol.edu.pk (Z.A.S.)

[2] School of Construction Management & Quantity Surveying, College of Engineering, Construction and Living Sciences, Otago Polytechnic, Dunedin 9016, New Zealand

* Correspondence: muhammad.alikhan@ce.uol.edu.pk (M.A.K.); rehan.masood@op.ac.nz (R.M.)

Abstract: In the local building industry of Pakistan, pre-engineered steel building manufacturers mainly employ their own self-developed software and Excel sheets. These systems are based on empirical formulas mentioned in the AISI manual. Under this scenario, a need was found to validate AISI flow charts using commercial software like CUFSM 5.04 and ABAQUS R2019x. This study presents a validation of the CUFSM software and the American Iron and Steel Institute (AISI) Direct Strength Method (DSM) results of channel section flexural members using the non-linear finite element method employing ABAQUS. In this study, eight standard cold-formed channel-section (C-section) steel members were modeled and analyzed using ABAQUS to simulate realistic behavior under four-point loading conditions. The non-linear finite element models incorporated material and geometric non-linearities to capture the actual response of the steel elements. The results obtained from ABAQUS were compared with those predicted by the CUFSM and DSM, focusing on critical parameters such as nominal strength, buckling modes, and deformation patterns. During this study, it was observed that out of the selected sections, the AISI charts predict conservative and even unsafe flexural capacities in some of the cases concerning other methods, with a maximum difference of 14.03%. The differences obtained using DSM and ABAQUS when compared with the results of the AISI charts varies on both the plus and minus sides. This study will not only affect the industry in terms of innovative designs for efficient structures but also the community in regards to low-budget construction.

Keywords: DSM; CUFSM; ABAQUS; local buckling; distortional buckling; global buckling; non-linear buckling; FEM

1. Introduction

In the past, cold-formed steel (CFS) was not well recognized due to a lack of awareness and familiarity with this product among professionals. Also, the perception of CFS was that it was less durable when compared with traditional hot-rolled steel. Designing with CFS is more complex due to factors such as local, distortional, and torsional buckling. However, the structural analysis and design of CFS sections have undergone significant progress in recent years, mainly due to the development of various analytical and numerical methods. Among them, the Direct Strength Method (DSM) has gained wide acceptance and is included in the North American Specification for the Design of Cold-Formed Steel Structural Members (AISI S100). The DSM offers a more rational and less conservative approach compared to traditional methods because it directly relates the strength of a CFS element to its elastic buckling behavior, which then can be translated to inelastic buckling behavior and finally, to plastic flexural capacity.

CUFSM (Constrained and Unconstrained Finite Strip Method) software, which implements DSM principles, is a powerful tool for determining the elastic buckling

characteristics of CFS cross-sections. It enables the elastic analysis of local, distortional, and global buckling modes and provides basic data for the application of DSM in design. While the CUFSM and DSM provide a robust framework for predicting the behavior of CFS members, it is critical to validate these analytical approaches against more comprehensive and detailed methods.

Non-linear finite element analysis (FEA) using software such as ABAQUS offers a high-fidelity approach to modeling the complex behavior of CFS sections under various loading conditions. By incorporating material and geometric non-linearities, FEA can capture the actual behavior of CFS members more accurately than linear analytical methods. Thus, validating CUFSM and DSM predictions using results obtained from non-linear FEA can increase confidence in these methods and ensure their reliability in practical design applications.

Cold-formed steel elements are thin, light, and cost-effective. However, this efficiency comes with complications. Engineers must account for cross-sectional instability (i.e., local and distortional), in addition to the global buckling of the member [1]. The Direct Strength Method does not use effective width or iteration to determine the strength of the element for design. Instead, the designer must calculate the elastic buckling load for three cases of behavior: local, distortional, and global. These data, combined with the load that causes the first yield, are then analyzed and used to "directly" provide strength using simple prediction equations [2]. In another study, the analysis was carried out using the four-point bending method. For a thin-walled beam with an open cross-section, where the load and support act at the shear center, it is not possible to eliminate the torsional moment load because the investigated beams are not perfect [3]. CUFSM is a useful tool for identifying buckling classes, i.e., global, distortional, local, and other deformations, and the constrained finite strip method can provide both modal decomposition and modal identification of the conventional finite strip solution [4]. Schafer and Adany created a cross-sectional model in CUFSM and an eigenvalue analysis was then performed to determine the expected imperfection modes. The CUFSM model was then exported to ABAQUS (via an input file) to run an eigenvalue buckling analysis using the same imperfection modes [5]. In developing the DSM, Yu and Schafer performed two series of bending tests and finite element analyses on different C- and Z-profiles including local buckling [6] and deformational buckling [7]. These series were aimed at isolating the local and biased modes used in DSM validation [8].

Artificial Intelligence techniques were also applied for the prediction of the axial capacity of cold-formed steel channel sections to compare the results with those of EWM and DSM, leading to proposed improvements in the AS/NZS 4600:2018 design equations [9–11].

The increasing use of back-to-back built-up cold-formed steel (CFS) channel beams, valued for their cost-effectiveness and higher load capacities, is evaluated. This evaluation involves 12 experimental tests and a non-linear finite element (FE) model. Flexural strength was also affected by screw spacing [12]. The flexural behavior of CFS four-limb built-up beams with both closed and open sections was investigated through experiments and FE modeling. Four-point bending tests reveal that the open-section beams have higher ultimate load capacity than closed-section beams, with local buckling as the failure mode. Validated FE models show that flexural moment capacity increases with thickness and web depth [13]. The buckling mode is a key factor that influences the bending strength of the specimens. Also, the finite element method (FEM) is a reliable tool to obtain quite accurate results in a reasonable amount of time [14] as an optimization framework for CFS members to maximize their flexure capacity through EC3. It was found that for the same amount of material, folded-flange and super-sigma sections have a higher flexural capacity enhancement of approx. 60% and 65%, respectively [15]. A simplified finite element model was defined to analyze stresses in the components. The Bending capacity and flexural behavior were investigated numerically by using FEM and through experimental evaluations. The moment capacity of the beams decreased as the compression flange's plate slenderness increased. The results were used to evaluate,

and propose modifications to, the Direct Strength Method (DSM) for cold-formed steel specialized beams prone to local buckling [16–18]. Cold-formed steel (CFS) upright sections were evaluated using finite element analysis and AI/ML techniques to predict normalized ultimate load and deflection. The finite element method (FEM) provided data for analysis, and the "feature selection" method identified key factors affecting flexural strength [19].

Cold-formed thin-walled C steel channel is not only being used as an independent member but also in composite form as a composite floor system [20].

Non-linear FEM results are effectively used to describe all the buckling modes. Key parameters like length, thickness, and geometric imperfections significantly impact the beams' behavior [21,22].

This study aims to validate the analytical approach of CUFSM and AISI DSM using the non-linear finite element method (FEM), employing ABAQUS for channel section flexural members. By conducting comparative analyses on eight different sections, this research evaluates the accuracy of DSM and CUFSM predictions for CFS beam sections. The findings will contribute to a better understanding of the strengths and limitations of these methods, ultimately leading to their effective application in the design of cold-formed steel structures.

2. Materials and Methods

The design approaches used are described in the following subsections:

2.1. DSM (Direct Strength Method) Analytical Approach

The Direct Strength Method (DSM) is an efficient and modern approach to the design of cold-formed steel structures. It simplifies the analysis and design process by directly calculating the strength of members, considering various limiting states such as local, distortional, and global buckling [23].

The American Iron and Steel Institute (AISI) Specification for the Design of Cold-Formed Steel Structural Members provides a set of formulas, tables, and charts for the design of CFS members [24,25].

2.1.1. Yielding and Lateral–Torsional Buckling

For doubly or singly symmetrical sections bending about a symmetric axis, the following formulas are used.

Elastic flexural buckling about the y-axis is determined as follows:

$$\sigma_{ey} = \frac{\pi^2 E}{\left(\frac{K_y L_y}{r_y}\right)^2} \tag{1}$$

$$\sigma_t = \frac{1}{A r_o^2} G J + \frac{\pi^2 E C_w}{\left(\frac{K_y L_y}{r_y}\right)^2} \tag{2}$$

$$F_{cre} = \frac{C_b r_o A}{S_f} \sqrt{\sigma_{ey} \sigma_t} \tag{3}$$

For $F_{cre} \geq 2.78 F_y$,

$$F_n = F_y \tag{4}$$

For $2.78 F_y > F_{cre} > 0.56 F_y$,

$$F_n = \frac{10}{9} F_y \left(1 - \frac{10 F_y}{36 F_{cre}}\right) \tag{5}$$

For $F_{cre} <= 0.56 F_y$,

$$F_n = F_{cre} \tag{6}$$

$$M_y = S_{fy} \, F_y \tag{7}$$

$$M_{ne} = S_f \, F_n \tag{8}$$

M_{ne} is to be taken as the minimum critical elastic buckling moment in flexural, torsional, or flexural-torsional buckling.

M_{ne} is allowed to be increased, considering inelastic reserve capacity, only in cases in which $M_{cre} > 2.78 \, M_y$.

$$M_{cre} = S_f \, F_{cre} \tag{9}$$

$$M_p = Z_f \, F_y \tag{10}$$

For $M_{cre} > 2.78 \, M_y$

$$M_{ne} = M_p - (M_p - M_y) \, \frac{\sqrt{M_y / M_{cre}} - 0.23}{0.37} \; <= M_p \tag{11}$$

For $M_{cre} <= 2.78 \, M_y$

$$M_{ne} = S_f \, F_n \tag{12}$$

2.1.2. Local Buckling Combined with Yielding and Global Buckling

For members without holes and having flat webs:

M_{crl} = Critical Elastic Buckling moment

$$M_{crl} = 342 \, S_f \quad \text{(SI units)} \tag{13}$$

$$\lambda_l = \sqrt{\frac{M_{ne}}{M_{crl}}} \tag{14}$$

For $\lambda_l < 0.776$,

$$M_{nl} = M_{ne} \tag{15}$$

For $\lambda_l > 0.776$,

$$M_{nl} = [1 - 0.15(M_{crl}/M_{ne})0.4](M_{crl}/M_{ne})0.4M_{ne} \tag{16}$$

Revised λ_l for consideration of inelastic reserve capacity,

$$\lambda_l = \sqrt{\frac{M_y}{M_{crl}}} \tag{17}$$

$$C_{yl} = Z_f \, . \, F \tag{18}$$

M_{nl} may be revised to include the inelastic reserve capacity for sections symmetric about the axis of bending if $\lambda_l <= 0.776$ and $M_{ne} >= M_y$, as follows:

$$M_{nl} = M_y + (1 - 1/C^2{}_{yl})(M_p - M_y) \tag{19}$$

2.1.3. Distortional Buckling (AISI)

If the flange has full or partial rotational restraint provided by a brace, panel, or sheathing, the rotational stiffness (K_ϕ) may be added to the solution to employ a more detailed method mentioned in the AISI Commentary Section 2.3.3.3. The simplified method for unrestrained C and Z sections with simple lip stiffeners was used for the present study.

Outer depth, $h_o = h + t$;

Outer width, $b_o = b + t/2$ (without lips) and $b + t$ (with lips).

This method is applicable under the following limitations:

$$\begin{aligned}
&50 \leq h_o/t \leq 200; \\
&25 <= b_o/t <= 100; \\
&6.25 <= D/t <= 50; \\
&45° <= \theta <= 90°; \\
&2 <= h_o/b_o <= 8; \\
&0.04 <= D\sin\theta/b_o <= 0.5.
\end{aligned} \tag{20}$$

$$\beta = 1.0 \text{ for } L_m >= L_{cr} \tag{21}$$

$$\beta = 1.0 <= 1 + 0.4 (L/L_m)^{0.7} (1 + M1/M2)^{0.7} <= 1.3 \tag{22}$$

$$F_{crd} = \beta \, K_d \{\pi^2 E/12(1 - v^2)\}(t/b_o)^2 \tag{23}$$

$$M_{crd} = S_f \, F_{crd} = \text{Critical distortion buckling moment} \tag{24}$$

$$\lambda_d = \sqrt{\frac{M_y}{M_{crd}}} \tag{25}$$

$$\text{For } \lambda_d <= 0.673, \, M_{nd} = M_y \tag{26}$$

$$\text{For } \lambda_d > 0.673, \, M_{nd} = \{1 - 0.22 \, (M_{crd}/M_y)^{0.5}\} \, (M_{crd}/M_y)^{0.5} \, M_y \tag{27}$$

Revised λ_d for consideration of in elastic reserve capacity,

$$\lambda_d = \sqrt{\frac{M_y}{M_{crd}}} \tag{28}$$

$$C_{yd} = \sqrt{\frac{0.673}{\lambda_d}} <= 0.3 \tag{29}$$

$$M_p = Z_f \, F_y \tag{30}$$

M_{nd} may be revised to include the inelastic reserve capacity for sections symmetric about the axis of bending if $\lambda_d <= 0.673$, as follows:

$$M_{nd} = M_y + (1 - 1/C^2{}_{yd}) \, (M_p - M_y) \tag{31}$$

2.2. CUFSM

CUFSM (Constrained and Unconstrained Finite Strip Method) is a powerful tool used for the analysis and design of cold-formed steel (CFS) structures. Developed by Ben Schafer in 1997, CUFSM is widely recognized for its capabilities in evaluating the stability and performance of thin-walled structural members, which are critical components in modern construction. CUFSM is primarily used to performing following tasks:

- Analyzing the local, distortional, and global buckling behavior of thin-walled sections.
- Determining the elastic buckling loads and modes of CFS members.
- Aiding in the design and optimization of CFS sections by providing insights into their stability characteristics.

CUFSM utilizes the finite strip method (FSM), which is particularly efficient for analyzing prismatic (constant cross-section) members. FSM divides the structure into strips along its length, simplifying the calculation of buckling modes and loads.

2.3. ABAQUS
2.3.1. General

ABAQUS is a comprehensive and powerful suite of finite element analysis (FEA) software applications, widely used for simulating the physical behavior of structures under various

conditions. The finite element (FE) software ABAQUS was employed to create a finite element model (FEM) of CFS (cold-formed steel) channel sections. This tool has been effectively used for linear and non-linear analysis in past. The FEM included the measured dimensions of the specimens, initial geometric imperfections, and non-linear material properties. The analysis of the FEM was carried out in two distinct steps. The first step was used for linear perturbation analysis to obtain the buckling modes (Model-1), whereas during the second step, the "general static" method was applied for calculation of the moment capacity (Model-2).

2.3.2. Geometry Modeling and Material Properties

Linear buckling analysis is performed as the first phase of numerical investigations. For this, eight AISI standard sections were modeled in ABAQUS, as per their geometric properties. The following are the key features of the materials and properties used for this study:

(1)   Material grade, F_y = 380 MPa (55 ksi);
(2)   Modulus of elasticity, E = 200 GPa (29,500 ksi);
(3)   Poison ratio = 0.3;
(4)   Unbraced length for torsional buckling = L/3.

The length for each investigated section is taken from AISI Chart-II-1. The loads are applied at the L/4 distance from each end. To control the torsional buckling, lateral supports are provided at a spacing of L/3, and to control the general torsional effects, the loads are applied at the shear center.

Two shell extruded sections are defined, one for the main channel section and the other for flat plate attached at the back of the channel.

2.3.3. Element Type and Mesh Size

The shell elements are chosen for both the main channel sections and for the plate attached at the back of channel. To initiate the analysis step, eight eigenvalues were requested, with 16 vectors and 300 maximum iterations.

In this model, typically, the S4R element was used for meshing because of its effectiveness in capturing the behavior of structures such as plates, shells, and other thin-walled members. The S4R designation indicates a four-node doubly curved thin or thick shell element with reduced integration and hourglass control.

To control mesh size sensitivity, initially, a coarser mesh size of 1 mm was provided, and finally, 0.25 mm was chosen for convergence with minimum computing effort. To perform the Riks analysis, a minimum of one eigenvalue is required; however, eight eigenvalues were used in this study because this number was sufficient to capture all buckling modes in relatively less time.

2.3.4. Boundary Conditions and Loading Procedure

For this research work, simply supported boundary conditions were applied at both ends relative to the major axis bending. Laterally, roller supports were provided at both ends and at the L/3 distance intermediately.

Two unit point loads were applied at the L/4 distance from the ends. To avoid the twisting moments, loads were applied at the shear center. To achieve this, a flat plate of 5 mm thickness was attached to the back of the main C-section, along the depth of the section. The width of this plate was set equal to the distance from the shear center to the outer edge of the web.

2.3.5. Initial Geometric Imperfections Modeling

After the successful completion of step 1, the first eigenvalue was noted. The same model (Model-1) was copied as Model-2, and the following changes were made to it:

The material properties were modified for step 2 (non-linear analysis), as shown below.
For the plastic material properties, the parameters include:

i.   Yield stress = 380 MPa (55 ksi); plastic strain = 0;
ii.   Yield stress = 517 MPa (75 ksi); plastic strain = 0.2.

Then, the first eigenvalue noted in Model-1 was applied as a point load in Model-2. The boundary conditions were kept the same for the non-linear analysis; however, this step required the use of the modified Static-Riks method, thus mandating that the boundary conditions be assigned again.

The Static-Riks step in ABAQUS is specialized type of analysis step used for solving non-linear problems, particularly those involving instability phenomena such as buckling or snap-through behavior; it is also used for the post-buckling behavior of structures. This approach is also known as the arc-length method. The Static-Riks step is primarily used for buckling analysis to capture the post-buckling behavior of structures.

In the next step, the Model-2 input file keywords were modified with some additional text to capture the first mode behavior of Model-1. The following texts were added by using Model-2's Edit Keywords command at a specified location.

*IMPERFACTION, FILE = JOB-1, STEP = 1

1, 0.6

Then, the new job was created and submitted for analysis. Finally, the results were monitored to determine the critical buckling load.

2.3.6. Convergence Criterion

In linear buckling analysis, ABAQUS determines the critical load factors and the associated buckling modes. The process involves performing a linear eigenvalue analysis to find the load multiplier at which buckling occurs. Since this is a linear analysis, there are no iterative convergence criteria such as those used in non-linear analysis.

For non-linear buckling analysis using the Static-Riks method, automatic incrementation is used, and the arc length increments are provided by fixing the minimum and maximum limits for the estimated total arc length to achieve convergence. The values used in the present analysis are as follows:

- Maximum number of increments = 500;
- Arc length increments—initial = 0.01, minimum = 1×10^{-5}, maximum = 1×10^{36};
- Estimated total arc length = 1.

Automatic incrementation allows ABAQUS to dynamically adjust the arc length increment based on the convergence behavior during the analysis. This method provides greater flexibility and can handle complex non-linearities in a better way.

2.4. Sections Selected for the Study

A typical pre-engineered steel structure building partially utilizing cold formed sections is shown in Figure 1. The sections shown in Table 1 were selected to evaluate the buckling strengths. The lengths were taken from AISI Chart-II-1. The stress-strain curve for the steel used in this study is given in Figure 2 and the selected sections are graphically shown in Figure 3. These sections are standard AISI sections, while the thicknesses are selected to reflect those used in the local fabrication market of Pakistan.

Table 1. Standard sections and corresponding investigated lengths.

S/No	Standard Section Designation SI (FPS)	Length (L) from AISI Chart-II-1 mm (Inches)	Braced Length at L/3 mm (Inches)
1	203CS64 × 2.7 (8CS2.5 × 105)	1600.0 (63.0)	533.34 (21.00)
2	203CS64 × 2.2 (8CS2.5 × 085)	1930.4 (76.0)	643.47 (25.34)
3	203CS64 × 1.8 (8CS2.5 × 070)	2082.8 (82.0)	694.27 (27.34)
4	203CS64 × 1.7 (8CS2.5 × 065)	2082.8 (82.0)	694.27 (27.34)

Table 1. *Cont.*

S/No	Standard Section Designation SI (FPS)	Length (L) from AISI Chart-II-1 mm (Inches)	Braced Length at L/3 mm (Inches)
5	152CS64 × 2.7 (6CS2.5 × 105)	1397.0 (55.0)	465.67 (18.34)
6	152CS64 × 2.2 (6CS2.5 × 085)	1701.8 (67.0)	567.27 (22.34)
7	152CS64 × 1.8 (6CS2.5 × 070)	1790.7 (70.5)	596.90 (23.50)
8	152CS64 × 1.6 (6CS2.5 × 065)	1778.0 (70.0)	592.67 (23.34)

Figure 1. Steel building constructed using cold-formed steel channel sections.
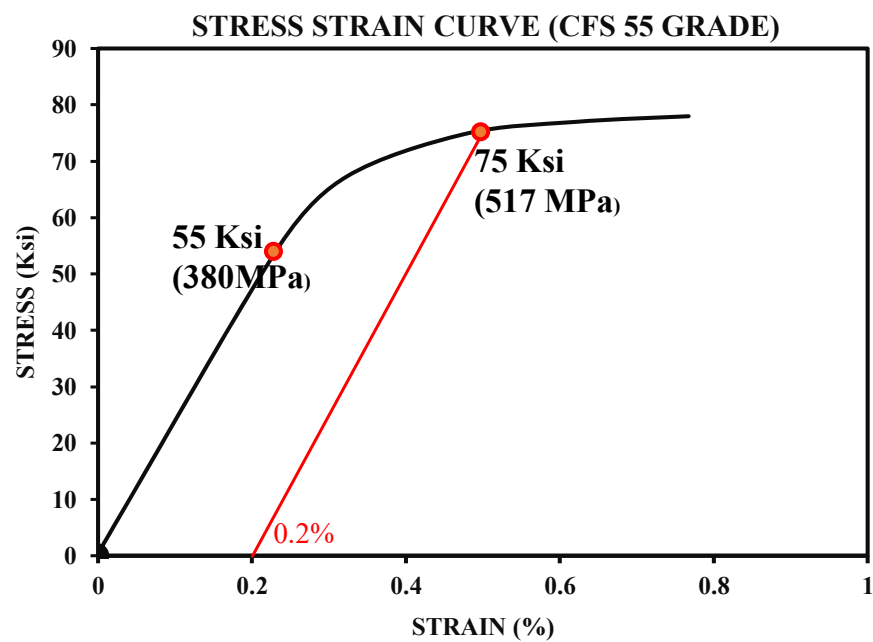
Figure 2. Stress–strain curve of cold-formed steel.
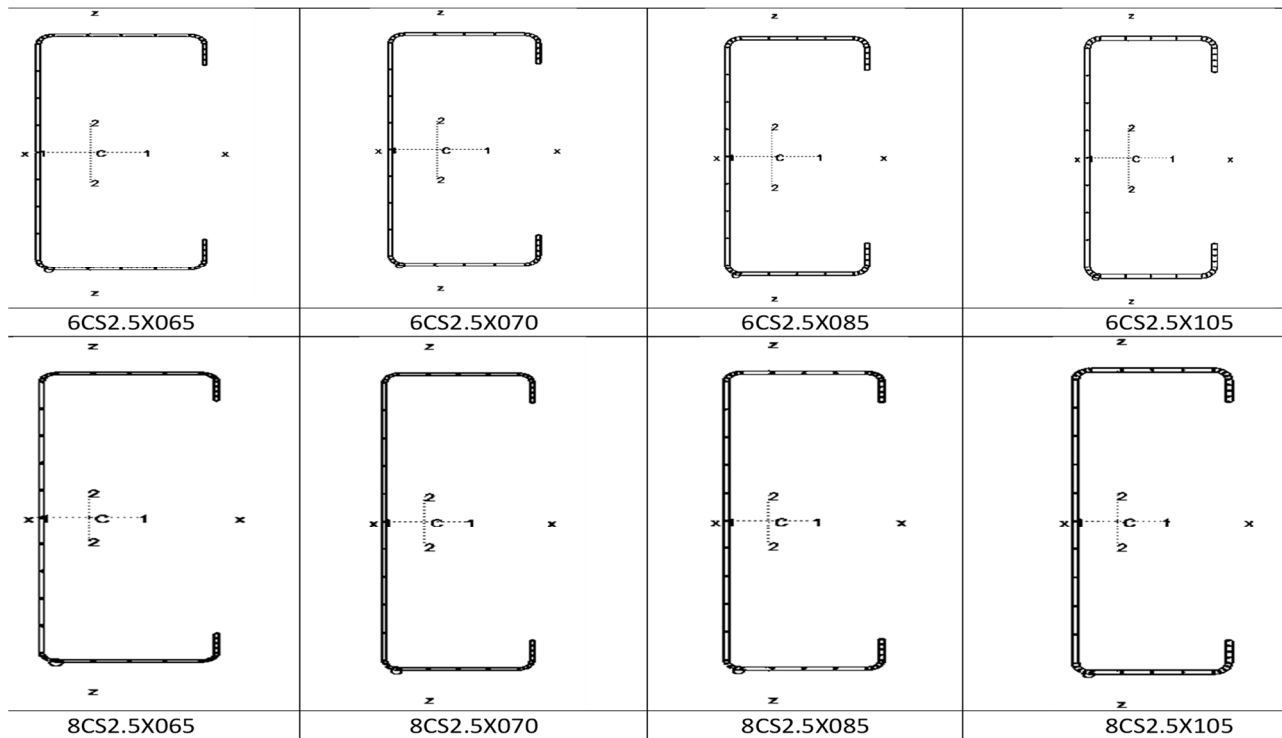
Figure 3. Investigated sections.

3. Results

3.1. Analytical

The DSM results were obtained using the expressions of Section 2.1, employing Excel sheets. The results are presented in Table 2.

Table 2. DSM flexural capacities of selected sections.

S/No	Section	M_{cre} kN-m (kip-in)	M_{crl} kN-mm (kip-in)	M_{crd} kN-m (kip-in)		M_{ne} kN-m (kip-in)	M_{nl} kN-m (kip-in)	M_{nd} kN-m (kip-in)
				Detailed Method	Approx. Method			
1	203CS64 × 2.7 (8CS2.5 × 105)	22.32 (197.50)	20.03 (177.30)	39.38 (348.50)	22.68 (200.74)	21.98 (194.50)	**18.32** **(162.10)**	20.98 (185.70)
2	203CS64 × 2.2 (8CS2.5 × 085)	18.13 (160.40)	16.34 (144.60)	24.11 (213.40)	13.47 (119.20)	18.15 (160.60)	**14.90** **(131.90)**	15.62 (138.20)
3	203CS64 × 1.8 (8CS2.5 × 070)	15.01 (132.80)	13.50 (119.50)	15.48 (137.00)	8.38 (74.20)	15.01 (132.80)	12.31 (108.90)	**11.83** **(104.70)**
4	203CS64 × 1.7 (8CS2.5 × 065)	13.94 (123.40)	12.55 (111.10)	13.09 (115.80)	7.01 (62.00)	13.94 (123.40)	11.47 (101.30)	**10.63** **(94.10)**
5	152CS64 × 2.7 (6CS2.5 × 105)	15.14 (134.00)	13.63 (120.60)	31.87 (282.00)	18.83 (166.60)	15.14 (134.00)	**12.43** **(110.00)**	14.95 (132.30)
6	152CS64 × 2.2 (6CS2.5 × 085)	12.35 (109.30)	11.11 (98.30)	19.70 (174.30)	11.21 (99.20)	12.35 (109.30)	**10.14** **(89.70)**	11.27 (99.70)

Table 2. *Cont.*

S/No	Section	M_{cre} kN-m (kip-in)	M_{crl} kN-mm (kip-in)	M_{crd} kN-m (kip-in)		M_{ne} kN-m (kip-in)	M_{nl} kN-m (kip-in)	M_{nd} kN-m (kip-in)
				Detailed Method	Approx. Method			
7	152CS64 × 1.8 (6CS2.5 × 070)	10.23 (90.50)	92.10 (81.50)	12.74 (112.70)	6.99 (61.90)	10.23 (90.5)	**8.40** **(74.30)**	8.61 (76.2)
8	152CS64 × 1.6 (6CS2.5 × 065)	9.51 (84.20)	8.57 (75.80)	10.79 (95.50)	5.84 (51.70)	9.51 (84.20)	7.81 (69.10)	**7.76** **(68.70)**

Bold values indicate the governing or minimum global, local, and distortional buckling strengths.

3.2. CUFSM

Linear buckling analysis is performed for the selected eight sections using CUFSM software, and the results are tabulated in Table 3:

Table 3. CUFSM flexural capacities of selected sections.

S/No	Section	M_{cre} kN-m (Kip-in)	Unbraced Length mm (Inches)	M_{crl} kN-m (Kip-in)	L_{crl} for $(M_{crl})_{min}$ mm (Inches)	M_{crd} kN-m (Kip-in)	L_{crd} for $(M_{crd})_{min}$ mm (Inches)
1	203CS64 × 2.7 (8CS2.5 × 105)	36.78 (325.50)	1600.0 (63.0)	58.90 (521.14)	101.6 (4.0)	44.83 (396.70)	533.40 (21.00)
2	203CS64 × 2.2 (8CS2.5 × 085)	19.84 (175.60)	1930.4 (76.0)	30.18 (267.10)	101.6 (4.0)	26.52 (234.70)	508.00 (20.00)
3	203CS64 × 1.8 (8CS2.5 × 070)	13.96 (123.50)	2082.8 (82.0)	16.87 (149.30)	101.6 (4.0)	17.45 (154.40)	694.40 (27.34)
4	203CS64 × 1.7 (8CS2.5 × 065)	13.34 (118.00)	2082.8 (82.0)	13.61 (120.40)	101.6 (4.0)	14.53 (128.60)	694.40 (27.34)
5	152CS64 × 2.7 (6CS2.5 × 105)	31.30 (277.00)	1397.0 (55.0)	57.32 (507.30)	76.2 (3.0)	35.02 (309.90)	465.80 (18.34)
6	152CS64 × 2.2 (6CS2.5 × 085)	17.65 (156.20)	1701.8 (67.0)	31.14 (275.60)	76.2 (3.0)	21.79 (192.80)	508.00 (20.00)
7	152CS64 × 1.8 (6CS2.5 × 070)	12.90 (114.10)	1778.0 (70.0)	17.56 (155.40)	76.2 (3.0)	14.13 (125.00)	592.80 (23.34)
8	152CS64 × 1.6 (6CS2.5 × 065)	12.43 (110.00)	1778.0 (70.0)	14.75 (130.50)	76.2 (3.0)	12.37 (109.50)	592.80 (23.34)

3.3. ABAQUS

In ABAQUS, a Load Proportionality Factor (LPF) vs. Arc Length graph is a crucial post-processing tool used in non-linear analysis, particularly for studying the stability and post-buckling behavior of structures. This graph is generated when performing analyses such as the Riks analysis (arc-length method), which is used to trace the equilibrium path of structures through points of instability.

The LPF is a scalar multiplier that scales the applied loads. An LPF of 1 means that the full applied load is active, while values greater than 1 indicate loads greater than the initial applied loads, and values less than 1 indicate partial loading. It helps to understand how the structure responds to different levels of loading and to identify the maximum load-carrying capacity.

Arc length is a measure of the progress of the analysis along the equilibrium path. It is not a physical length but a parameter that controls the progress of the load and displacement in non-linear analyses. It allows the analysis to continue through points

where the structure exhibits snap-through or snap-back behavior, ensuring that a complete load-displacement path is traced. At a later stage, the arc length may be scaled to any displacement. The load-deflection curves obtained, along with the failure mode for all samples, are shown in Figures 4–11.
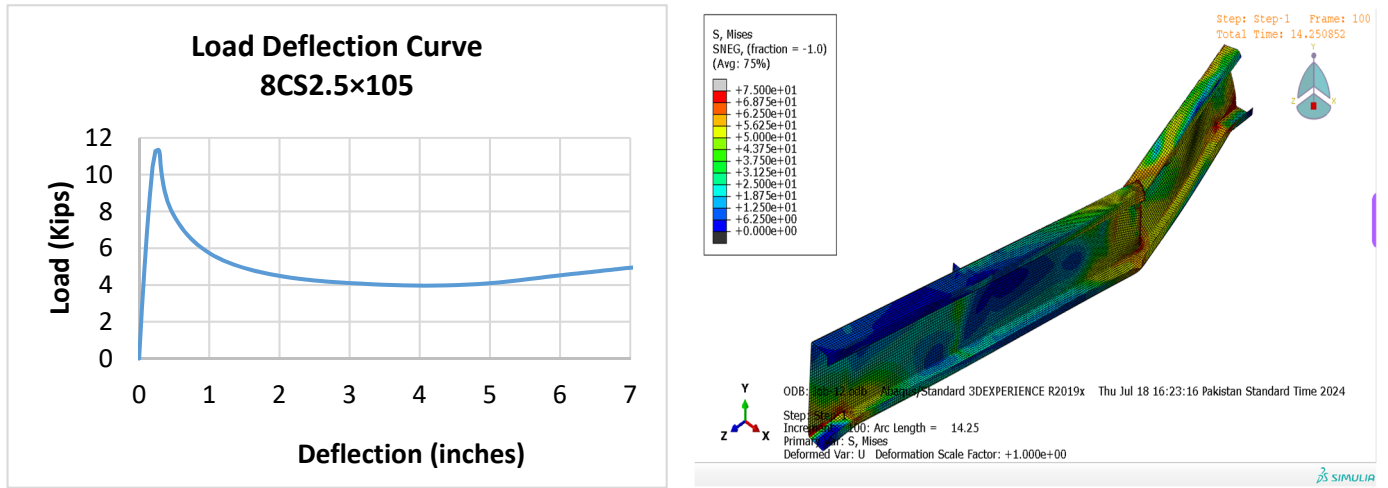

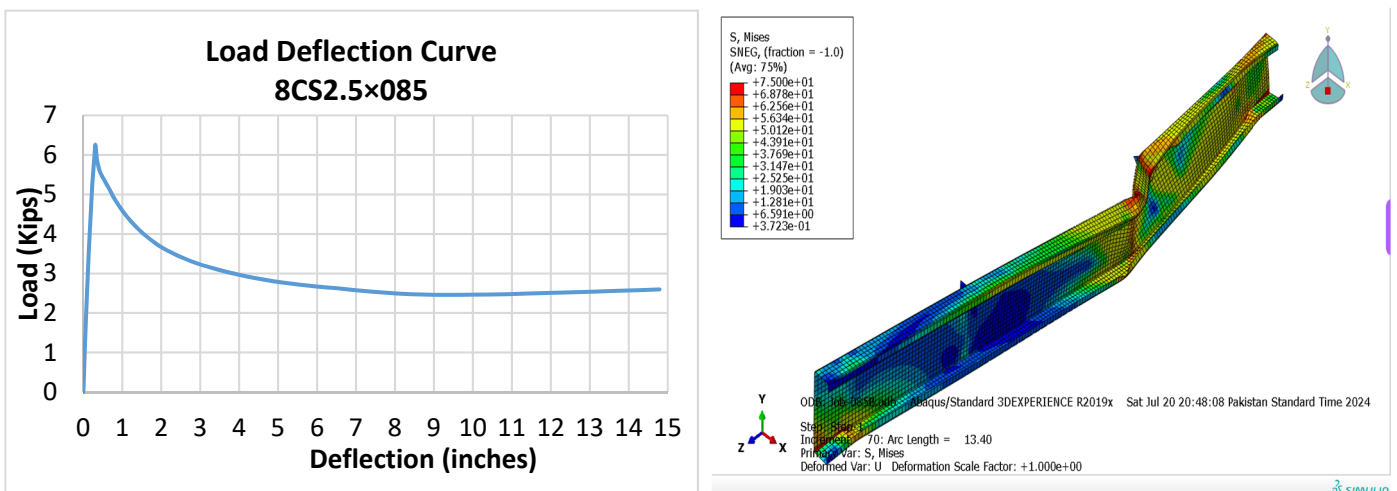**Figure 4.** Load vs. deflection graph for section 8CS2.5 × 105 and deformed shape.

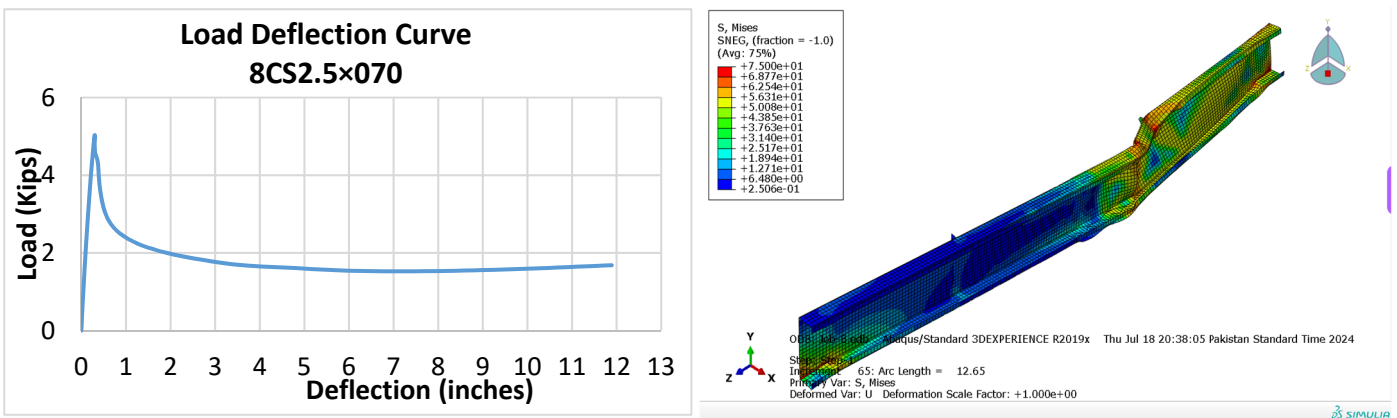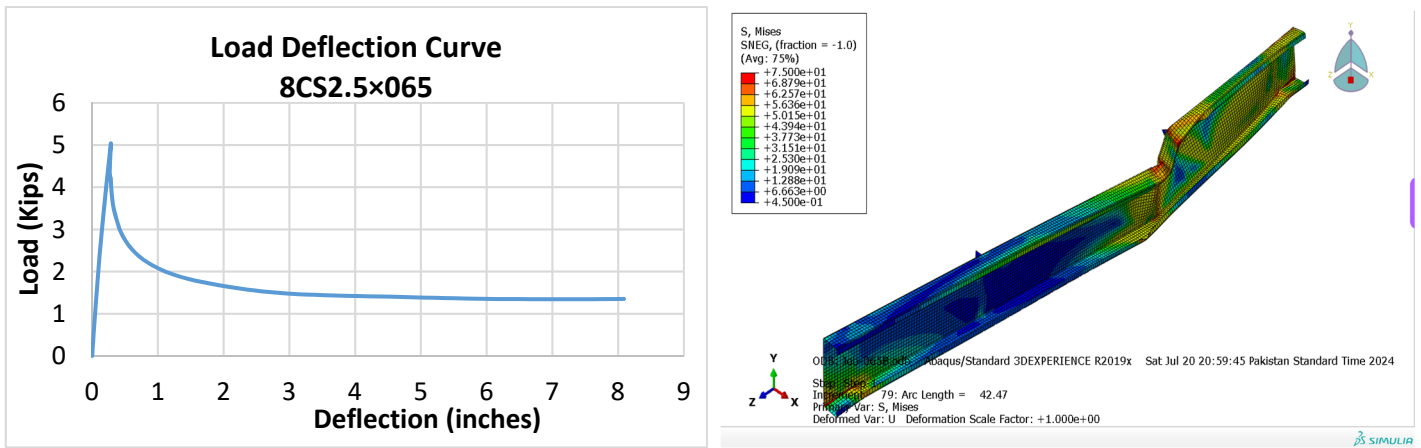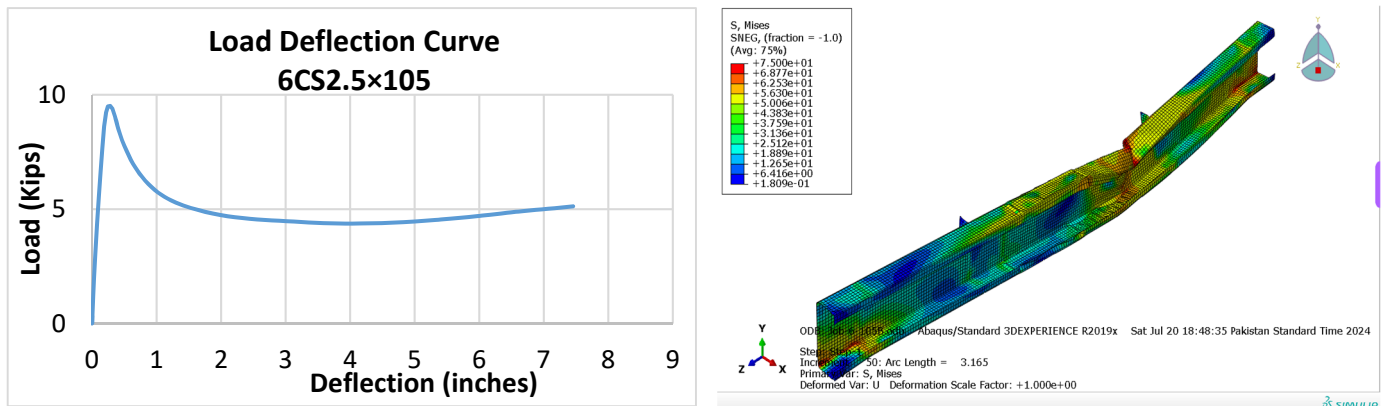**Figure 5.** Load vs. deflection graph for section 8CS2.5 × 085 and deformed shape.

Figure 6. Load vs. deflection graph for section 8CS2.5 × 070 and deformed shape.

Figure 7. Load vs. deflection graph for section 8CS2.5 × 065 and deformed shape.

Figure 8. Load vs. deflection graph for section 6CS2.5 × 105 and deformed shape.

Following are the salient features of these plots:

- *X*-axis—This represents the vertical deflection under the load point near the roller support. Similarly, LPF may be translated into the load at any stage.
- *Y*-axis (Load Proportionality Factor)—This represents the scaling of the applied load.
- Ascending branch—This indicates that the structure is carrying an increasing load, without significant deformation. This typically corresponds to the elastic behavior of the structure.
- Peak point—The highest point on the plot represents the maximum load-carrying capacity of the structure. Beyond this point, the structure may undergo buckling or failure.
- Descending branch—If the plot shows a descending branch after the peak, it indicates post-buckling or post-failure behavior. The structure might still carry the load but with significant deformations.
- Post-buckling strength—After very large deformations, some extra post-buckling strength is obtained due to intermediate falsely stable configurations, and the load–deflection curve moves slightly upwards [26,27].

After gathering the LPF data for each investigated section, the nominal moment capacities are calculated and tabulated, as shown in Table 4.
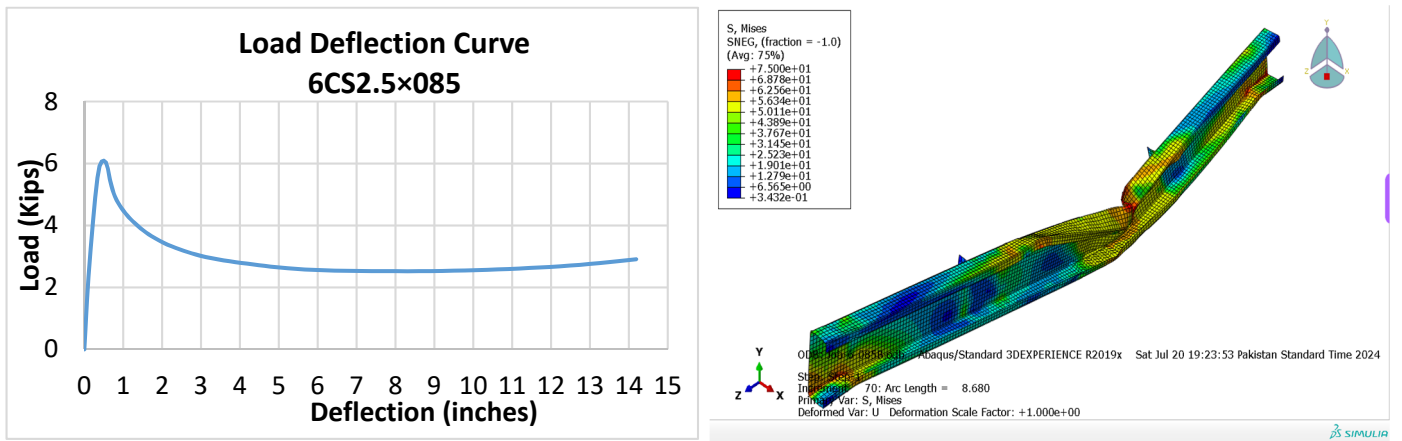
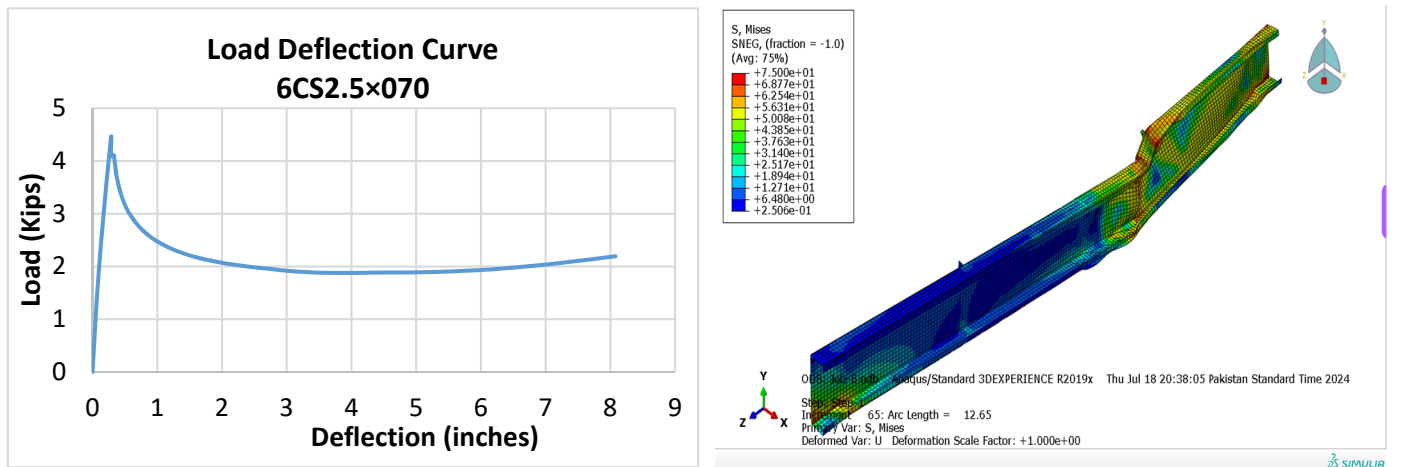**Figure 9.** Load vs. deflection graph for section 6CS2.5 × 085 and deformed shape.

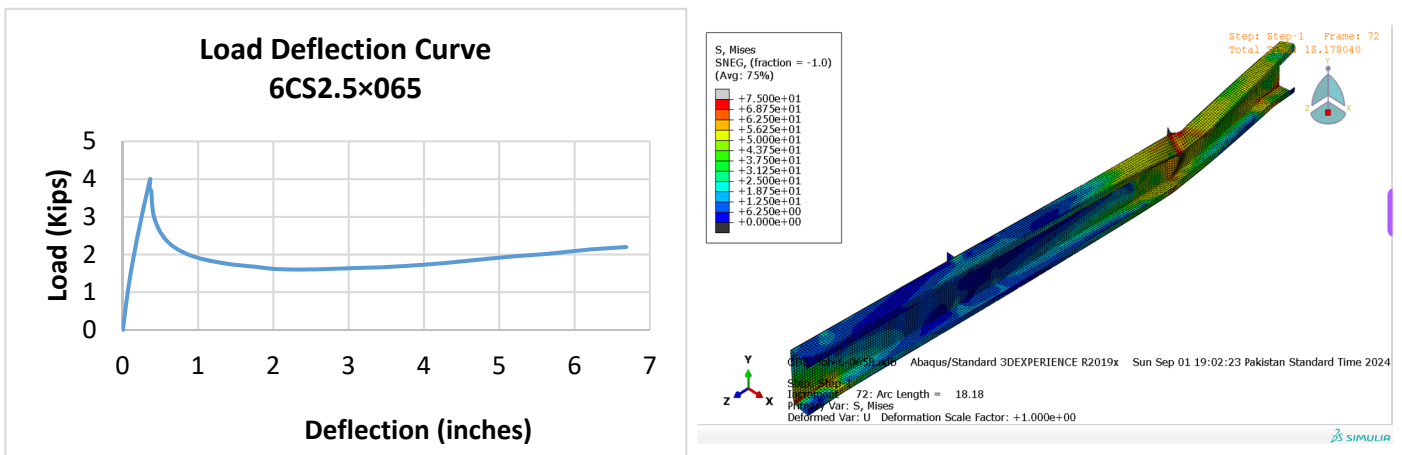**Figure 10.** Load vs. deflection graph for section 6CS2.5 × 070 and deformed shape.

Figure 11. Load vs. deflection graph for section 6CS2.5 × 065 and deformed shape.

Table 4. ABAQUS flexural capacities of selected sections.

| S/No	Section	M_n N-mm (Kip-in)
1	203CS64 × 2.7 (8CS2.5 × 105)	19,413,400 (171.8)
2	203CS64 × 2.2 (8CS2.5 × 085)	14,546,490 (128.7)
3	203CS64 × 1.8 (8CS2.5 × 070)	11,243,500 (99.5)
4	203CS64 × 1.7 (8CS2.5 × 065)	11,537,300 (102.1)
5	152CS64 × 2.7 (6CS2.5 × 105)	14,452,700 (127.9)
6	152CS64 × 2.2 (6CS2.5 × 085)	11,492,100 (101.7)
7	152CS64 × 1.8 (6CS2.5 × 070)	8,904,400 (78.8)
8	152CS64 × 1.6 (6CS2.5 × 065)	7,797,000 (69.0)

3.4. Comparison

The AISI chart, the AISI DSM method, CUFSM, and ABAQUS nominal strengths for non-linear buckling are compared; the evaluation is shown in Table 5.

Table 5. Comparison between the AISI chart, AISI DSM, CUFSM, and ABAQUS.

S/No	Section	AISI CHART M_n kN-m (kip-in)	DSM M_n kN-m (kip-in)	Percentage Difference with AISI CHART (%)	ABAQUS M_n kN-m (kip-in)	Percentage Difference with AISI CHART (%)	CUFSM M_n kN-m (kip-in)	Percentage Difference with AISI CHART (%)
1	203CS64 × 2.7 (8CS2.5 × 105)	19.89 (176.00)	18.32 (162.10)	−8.57	19.41 (171.80)	−2.47	21.76 (192.61)	+9.44
2	203CS64 × 2.2 (8CS2.5 × 085)	14.80 (131.00)	14.90 (131.90)	+0.68	14.55 (128.73)	−1.72	16.11 (142.53)	+8.80
3	203CS64 × 1.8 (8CS2.5 × 070)	11.27 (99.70)	11.83 (104.70)	+4.97	11.24 (99.50)	−0.27	12.34 (109.21)	+9.54
4	203CS64 × 1.7 (8CS2.5 × 065)	10.12 (89.60)	10.63 (94.10)	+5.04	11.54 (102.10)	+14.03	11.04 (97.7)	+9.04
5	152CS64 × 2.7 (6CS2.5 × 105)	14.13 (125.00)	12.43 (110.00)	−13.68	14.45 (127.90)	+2.26	14.88 (131.69)	+5.35
6	152CS64 × 2.2 (6CS2.5 × 085)	10.66 (94.30)	10.14 (89.70)	−5.13	11.49 (101.70)	+7.79	11.61 (102.73)	+8.94
7	152CS64 × 1.8 (6CS2.5 × 070)	8.16 (72.20)	8.40 (74.30)	+2.89	8.90 (78.80)	+9.07	8.91 (78.86)	+9.22
8	152CS64 × 1.6 (6CS2.5 × 065)	7.36 (65.10)	7.76 (68.70)	+5.43	7.80 (69.00)	+5.98	8.13 (71.93)	+10.49

The results of Table 5 are graphically shown in Figure 12. The comments regarding the results shown in Table 5 are given below:

1. The DSM results are in relatively good agreement with the AISI chart, with percentage differences ranging from −8.57% to +5.43%. The observed differences are likely due to the basic approximations in the DSM for predicting the strength of cold-formed steel sections.

2. ABAQUS provides a more detailed and potentially more accurate prediction of moment capacities. It is particularly useful for detailed analyses in which capturing complex behaviors is essential. In this study, the AISI chart values are closer to the ABAQUS results, with differences mainly within ±10%. The observed range of −2.47% to +14.03% shows that AISI charts can accurately predict the complex stress–strain behavior of steel sections.

3. CUFSM tends to predict higher moment capacities, with percentage differences ranging from +5.35% to +10.49%. This consistent overestimation suggests that AISI might have employed conservative assumptions for design purposes.
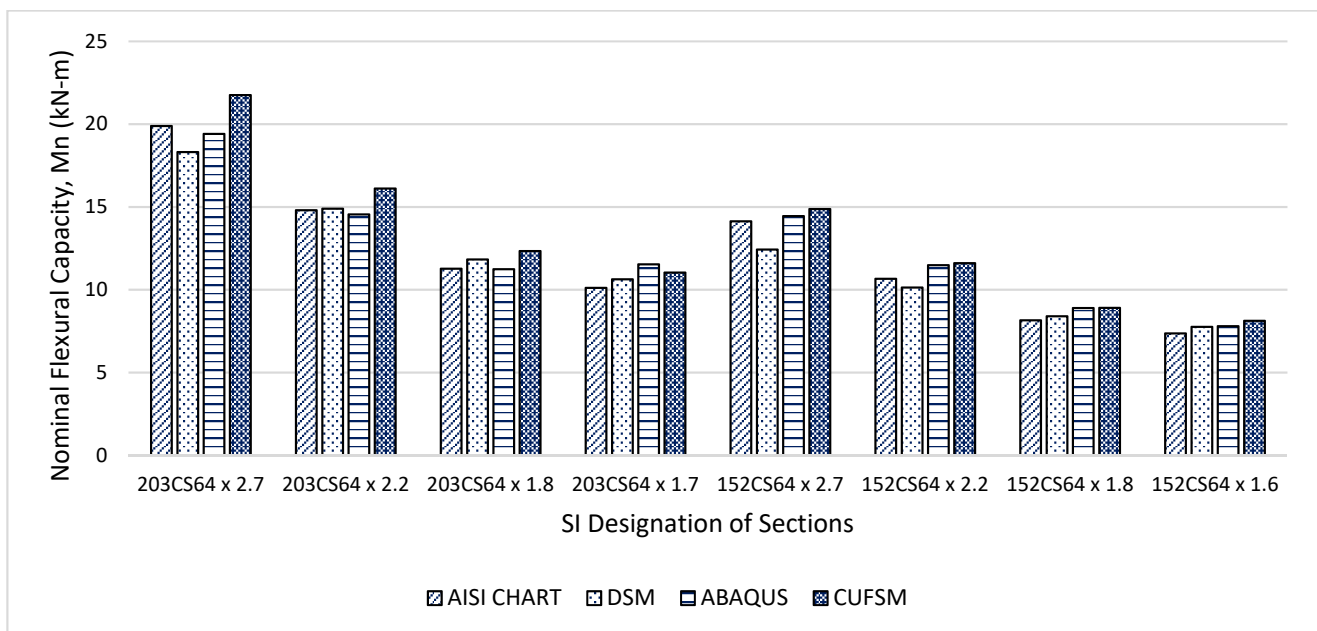
Figure 12. Comparison of nominal flexural capacities predicted by AISI charts, DSM, ABAQUS, and CUFSM.

4. Conclusions

In this paper, a comparative study is conducted on eight selected CFS channel members. To control torsion, loads are applied at the shear center of each respective section, and to control torsional buckling, bracing is provided at a regular interval of L/3. The four-point bending method is adopted.

Manual calculations are performed on the basis of the AISI DSM method to capture the non-linear buckling behavior. CUFSM is used to perform linear analysis, then these results are used to perform a non-linear analysis via DSM to identify the failure strengths. In ABAQUS, models are developed to perform a non-linear FEM analysis.

It is observed that the governing failure modes for all the eight specimens were local, distortional, and a combination of these modes. The results acquired by all three methods mentioned are compared with the AISI charts, and the following conclusions can be drawn:

1. The AISI charts can be used by designers with confidence for practical designs because of their conservative nature, in most cases. However, to achieve economy and for speedy design, the CUFSM software may be employed. For detailed design-

ing, when sufficient time is available, ABAQUS can provide economical, safe, and reliable solutions.

2. DSM is a scientifically sound method that aligns closely with the AISI chart, providing reliable predictions, with only minor discrepancies.
3. The ABAQUS finite element analysis results show a small to moderate deviation from the AISI charts, with percentage differences ranging from -2.47% to $+14.03\%$.
4. CUFSM consistently predicts higher moment capacities compared to those in the AISI charts, with positive percentage differences ranging from $+5.35\%$ to $+10.49\%$.
5. The difference between the DSM and ABAQUS flexural strength results with respect to the AISI charts varies on both the plus and minus sides.
6. In the selected sections, as the thickness decreases, the results from all the four approaches come closer to each other. This means that the thin wall behavior is captured well by all of these methods.
7. It is to be noted that for the selected sections and their specific unbraced lengths, AISI charts predict higher strengths for three out of eight sections when compared with the ABAQUS results, with a maximum difference of 2.47%.
8. The DSM values vary from those in the AISI charts on both the plus and minus sides, with a maximum difference of 13.68% and the charts being on the unsafe side.

List of Abbreviations

AI/ML	Artificial Intelligence/Machine Learning
AISI	American Iron and Steel Institute
AISI S100	North American Specifications for the Design of Cold-Formed Steel Structural Members
AS/NZS	Australian/New Zealand Standards
CFS	Cold-Formed Sections
CUFSM	Constrained and Unconstrained Finite Strip Method
DSM	Direct Strength Method
EC3	Euro Code 3
FE	Finite Element
FEA	Finite Element Analysis
FEM	Finite Element Method
FSM	Finite Strip Method
LPF	Load Proportionality Factor

Nomenclature

A	Full, unreduced cross-sectional area of member
C_b	Bending coefficient dependent on moment gradient
C_m	Coefficient assuming no lateral translation of frame
C_w	Warping constant of torsion
E	Modulus of elasticity of steel
F_{crd}	Elastic distortional buckling stress
F_{cre}	Critical elastic flexural, torsional, or flexural–torsional buckling stress
F_y	Yield stress
G	Shear modulus of steel
J	Saint-Venant's torsion constant of the cross-section (for open sections composed of n segments of uniform thickness).
K_d	Effective length factor for distortion 0.5 <= 0.1 (bo . D .Sinθ/ho . t)0.7 <= 8.0
K_t	Effective length factor for twisting
K_x	Effective length factor for bending about x-axis
K_y	Effective length factor for bending about y-axis
$k_{\phi fe}$	Elastic rotational stiffness provided the flange
$k_{\phi we}$	Elastic rotational stiffness provided by the web to the flange-web juncture
k_ϕ	Rotational stiffness provided by bracing to the flange-web juncture
$k{\sim}_{\phi fg}$	Geometric rotational stiffness demanded by the flange from the flange-web juncture
$k{\sim}_{\phi wg}$	Geometric rotational stiffness demanded by the web from the flange-web juncture
L	Span length
L_b	Distance between braces on individual concentrically loaded compression member to be braced
L_{cr}	Critical unbraced length of distortional buckling1.5 h_o (b_o $DSinθ/h_o$ t)0.6 <= 10 h_o
L_{crd}	Critical unbraced length of distortional buckling
L_{crl}	Critical unbraced length of local buckling
L_m	Distance between discrete restraints that restrict distortional or shear buckling
L_u	Limit of unbraced length below which lateral–torsional buckling is not considered
L_x	Unbraced length of member for bending about x-axis
L_y	Unbraced length of member for bending about y-axis
L_t	Unbraced length of member for torsion
M_{cr}	M_{cre}, global (lateral–torsional); M_{crl}, local; or M_{crd}, distortional elastic buckling moment about the axis of bending
M_{crd}	Distortional buckling moment
M_{cre}	Global buckling momentLateral–torsional buckling moment
M_{cr}	Critical elastic local buckling moment
M_n	Nominal flexural moment
M_{nd}	Nominal flexural moment for distortional buckling
M_{ne}	Nominal flexural moment for yielding and global (lateral–torsional) buckling
M_{nl}	Nominal flexural moment for local buckling
M_p	Member plastic moment
M_y	Member yield moment (=$S_{fy}F_y$)
$M1, M2$	Smaller and larger end moments in an unbraced segment, respectively, in the unbraced length, L_m; $M1/M2$ is positive for reverse curvature
r_o	Polar radius of gyration about the shear center
r_x	Radius of gyration of full unreduced cross-section about x-axis
r_y	Radius of gyration of full unreduced cross-section about y-axis
S_e	Effective section modulus calculated relative to extreme compression or tension fiber at $F_y$orEffective section modulus calculated at extreme fiber compressive stress of F_n
S_f	Elastic section modulus of full unreduced section relative to extreme compression
S_{fy}	Elastic section modulus of full unreduced cross-section relative to extreme fiber in first yielding
t	Base steel thickness of any element or section
Z_f	Plastic section modulus

β	A value accounting for moment gradient may be conservatively taken as 1.0
σ_{ey}	Elastic flexural buckling stress
σ_t	Torsional buckling stress

References

1. Li, Z.; Schafer, B.W. Buckling Analysis of Cold-formed Steel Members with General Boundary Conditions Using CUFSM Conventional and Constrained Finite Strip Methods. In Proceedings of the 20th International Specialty Conference on Cold Formed Steel Sections, St. Louis, MO, USA, 3–4 November 2010.
2. Naidu, G.M.; Patil, U.; Nandihalli, P.; Kothapally, T.H.; Devi, T.A.; Usanova, K.I. Comparison study on cold formed steel of coupled channel section based on abaqus and cufsm by simple-simple end condition. *MATEC Web Conf.* **2024**, *392*, 01010. [CrossRef]
3. Obst, M.; Wasilewicz, P.; Adamiec, J. Experimental investigation of four-point bending of thin walled open section steel beam loaded and set in the shear center. *Sci. Rep.* **2022**, *12*, 7275. [CrossRef]
4. Adany, S. Buckling Analysis of Cold-formed Steel Members Using CUFSM. In Proceedings of the 18th International Specialty Conference on Cold-Formed Steel Structures, Orlando, FL, USA, 26–27 October 2006.
5. Öztürk, F.; Mojtabaei, S.M.; Şentürk, M.; Pul, S.; Hajirasouliha, I. Buckling behaviour of cold-formed steel sigma and lipped channel beam–column members. *Thin-Walled Struct.* **2022**, *173*, 108963. [CrossRef]
6. Cheng, Y.; Schafer, B.W. Local buckling tests on cold-formed steel beams. *J. Struct. Eng.* **2003**, *129*, 1596–1606. [CrossRef]
7. Cheng, Y.; Schafer, B.W. Distortional Buckling Tests on Cold-Formed Steel Beams. *J. Struct. Eng.* **2006**, *132*, 515–528. [CrossRef]
8. Pham, C.H.; Hancock, G.J. Numerical simulation of high strength cold-formed purlins in combined bending and shear. *J. Constr. Steel Res.* **2010**, *66*, 1205–1217. [CrossRef]
9. Fang, Z.; Roy, K.; Mares, J.; Sham, C.-W.; Chen, B.; Lim, J.B. Deep learning-based axial capacity prediction for cold-formed steel channel sections using Deep Belief Network. *Structures* **2021**, *33*, 2792–2802. [CrossRef]
10. Dai, Y.; Roy, K.; Fang, Z.; Raftery, G.M.; Lim, J.B. Web crippling resistance of cold-formed steel built-up box sections through experimental testing, numerical simulation and deep learning. *Thin-Walled Struct.* **2023**, *192*, 111190. [CrossRef]
11. Dai, Y.; Fang, Z.; Roy, K.; Raftery, G.M.; Lim, J.B. Optimal design of cold-formed steel face-to-face built-up columns through deep belief network and genetic algorithm. *Structures* **2023**, *56*, 104906. [CrossRef]
12. Roy, K.; Lau, H.H.; Ting, T.C.H.; Chen, B.; Lim, J.B. Flexural behaviour of back-to-back built-up cold-formed steel channel beams: Experiments and finite element modelling. *Structures* **2021**, *29*, 235–253. [CrossRef]
13. Deng, F.; He, Y.; Deng, L.; Zhong, W. Experimental and Numerical Study on the Flexural Behavior of Cold-Formed Steel Multi-Limb Built-Up Section Beams. *Buildings* **2022**, *12*, 1639. [CrossRef]
14. Wang, H.; Zhang, Y. Experimental and numerical investigation on cold-formed steel C-section flexural members. *J. Constr. Steel Res.* **2009**, *65*, 1225–1235. [CrossRef]
15. Gatheeshgar, P.; Poologanathan, K.; Gunalan, S.; Nagaratnam, B.; Tsavdaridis, K.D.; Ye, J. Structural behaviour of optimized cold-formed steel beams. *Steel Constr.* **2020**, *13*, 294–304. [CrossRef]
16. Karthik, C.; Anbarasu, M. Cold-formed ferritic stainless steel closed built-up beams: Flexural behaviour and numerical parametric study. *Thin-Walled Struct.* **2021**, *164*, 107816. [CrossRef]
17. Cobo, M.M.; Alvarez, J.D.C.; de Hasbun, P.M.; Hasbun, J.C.H.; Amador, A.M.G.; de Cisneros, J.J.J. Experimental Behavior of a Full-Scale Housing Section Built with Cold-Formed Steel Shear Wall Panels under Horizontal Monotonic and Cyclic Loading. *Appl. Sci.* **2021**, *11*, 10934. [CrossRef]
18. Taheri, E.; Firouzianhaji, A.; Mehrabi, P.; Hosseini, B.V.; Samali, B. Experimental and Numerical Investigation of a Method for Strengthening Cold-Formed Steel Profiles in Bending. *Appl. Sci.* **2020**, *10*, 3855. [CrossRef]
19. Taheri, E.; Fard, S.E.; Zandi, Y.; Samali, B. Experimental and Numerical Investigation of an Innovative Method for Strengthening Cold-Formed Steel Profiles in Bending throughout Finite Element Modeling and Application of Neural Network Based on Feature Selection Method. *Appl. Sci.* **2021**, *11*, 5242. [CrossRef]
20. Liu, D.; Fu, F.; Liu, W. Structural Behavior of Composite Floor System Using Cold-Formed Thin-Walled C Steel Channel Embedded Foam Concrete. *Appl. Sci.* **2021**, *11*, 9888. [CrossRef]
21. Aktepe, R.; Erkal, B.G. Experimental and numerical study on flexural behaviour of cold-formed steel hat-shaped beams with geometrical imperfections. *J. Constr. Steel Res.* **2023**, *202*, 107774. [CrossRef]
22. Taheri, E.; Firouzianhaji, A.; Usefi, N.; Mehrabi, P.; Ronagh, H.; Samali, B. Investigation of a Method for Strengthening Perforated Cold-Formed Steel Profiles under Compression Loads. *Appl. Sci.* **2019**, *9*, 5085. [CrossRef]
23. Siddiqi, Z.A. *Steel Structures*, 4th ed.; Help Civil Engineering Publisher: Lahore, Pakistan, 2017.
24. Buckholt, J.; Chen, H. *The 2017 AISI Cold-Formed Steel Design Manual (2018)*; Missouri University of Science and Technology: Rolla, MO, USA, 2018.
25. American Iron and Steel Institute (AISI). *North American Specification for the Design of Cold-Formed Steel Structural Members*; AISI: Washington, DC, USA, 2016.

26. Schafer, B.W. Local, distortional, and Euler buckling of thin-walled columns. *J. Struct. Eng.* **2002**, *128*, 289–299. [CrossRef]
27. Shifferaw, Y.; Schafer, B.W. Inelastic Bending Capacity of Cold-Formed Steel Members. *J. Struct. Eng.* **2012**, *138*, 468–480. [CrossRef]